Appl. Phys. B 72, 207–213 (2001) / Digital Object Identifier (DOI) 10.1007/s003400000423

Applied Physics B
Lasers
and Optics

Fluorescence quantum yield of rhodamine 101 in the presence of absorption saturation

A. Marcano O.[1], **I. Urdaneta**[2]

[1] Centro de Física, Instituto Venezolano de Investigaciones Científicas, Caracas 1020 A, Apartado 21827, Venezuela
(E-mail: marcano@pion.ivic.ve)
[2] Departamento de Química, Universidad Simón Bolívar, Valle de Sartenejas, Caracas 1080 A, Venezuela

Received: 16 November 1999/Revised version: 5 July 2000/Published online: 13 September 2000 –

Abstract. Using the photothermal method we measure the fluorescence quantum yield of a rhodamine 101 solution in ethanol for different values of the pump-field fluence. Our experiments reveal a depletion of the fluorescence quantum yield as the pump fluence increases. To explain the observed fluorescence quenching, a dependence of the nonradiative relaxation rates on the field fluence is proposed. Predictions of the model are in good agreement with the experiments.

PACS: 33.50.-j; 33.50.Hv; 78.20.Nv

The thermal lensing (TL) method has been widely used for the determination of quantum yield of highly fluorescent dyes [1–5]. This method measures the amount of heat deposited in the medium after the absorption of the incident photons. In highly fluorescent dyes, such as rhodamines, a major part of the energy of the absorbed photons is converted into fluorescence. However, a smaller part of this energy is converted into heat through nonradiative relaxation mechanisms. By measuring this amount of energy and comparing it with the total energy lost, one can estimate the energy used for the fluorescence process.

The use of TL for measuring the fluorescence quantum yield makes it possible to study the influence of different factors, such as dye concentration, pump-field power and solvent properties. The quenching of the fluorescence due to light intensity has been studied widely [6–10]. Different mechanisms were suggested to explain the fluorescence quenching due to high light-intensity levels. Peretti and Ranson suggested that the fluorescence quenching in dye solutions resulted from the absorption of the pump light by the excited molecules to higher excited states, followed by a decay that bypasses the energy level associated with fluorescence [7]. Other authors claim that the quenching is the result of stimulated transitions to the lower levels [9, 10]. The role of absorption saturation has not been considered as a factor that can reduce the fluorescence quantum efficiency, although it limits the amount of molecules in the excited level. As the relative amount of excited molecules that relax through a nonradiative process will not be affected in the same way as the molecules contributing to the fluorescence, the probability of nonradiative transitions may change with saturating field fluences. Furthermore, as the probability of the fluorescence transition must remain constant, the efficiency of the fluorescence process could be affected.

The purpose of this work is to study the role of absorption saturation on the fluorescence quantum yield. By measuring the total absorption and the thermal absorption coefficient, the fluorescence quantum yield of rhodamine 101 solution in ethanol is determined at different pump-light fluence values. We demonstrate experimentally that even in the case of strong absorption saturation, the thermal absorption coefficient is not affected. The total absorption reduces and stabilizes around the level of the thermal absorption. In this situation, all of the absorbed photons relax through the nonradiative channel, while the fluorescence emission quenches.

To understand these observations, we study the saturation of the absorption in a dye solution using a model that includes the two channels of possible relaxation from the excited state: the fluorescence and the nonradiative relaxation channels. The model suggests that the probability of the nonradiative relaxation increases with the field power and that the probability of the fluorescence transition remains constant. The results of the model are in good agreement with the observed experimental facts.

1 Method

We determine the fluorescence quantum yield using the expression [1]

$$\phi_{\mathrm{f}} = \frac{\langle \lambda_{\mathrm{f}} \rangle}{\lambda_{\mathrm{L}}} \left[1 - \frac{P_{\mathrm{th}}}{P_{\mathrm{L}} - P_{\mathrm{t}}} \right], \tag{1}$$

where λ_{L} is the laser wavelength, $\langle \lambda_{\mathrm{f}} \rangle$ is the mean fluorescence emission wavelength, P_{L} is the incident laser power, P_{t} is the laser power transmitted through the sample and P_{th} is the light power converted to heat. We define the total absorp-

tion coefficient through Beer's law:

$$\alpha = \frac{1}{L} \ln\left(\frac{P_L}{P_t}\right) , \tag{2}$$

where L is the length of the sample cell.

P_{th} is proportional to the phase shift induced in the medium due to the local heating of the sample. We measure this induced thermal phase shift by using a pump–probe Z-scan technique [11–15]. As shown below, this method is appropriate when a strong saturation of absorption is present. In our experiment, a fast pump pulse induces a thermal lens within the medium. A collinearly propagating probe beam tests this thermal lens. The changes of the probe-field transmission over a small aperture located at the far field measure the magnitude of the induced phase shift. The change of the refractive index due to the local heating of the sample is

$$\Delta n = \frac{F\alpha_{th}}{2\varrho C_V}\left(\frac{dn}{dT}\right) , \tag{3}$$

where F is the pump-field fluence, ϱ is the solvent density, C_V is the solvent heat capacity, dn/dT is the thermal gradient of the refractive index and α_{th} is the thermal absorption coefficient that accounts only for the energy lost in the heating process. α_{th} is related to P_{th} through the equation

$$\alpha_{th} = \frac{1}{L} \ln\left(\frac{P_L}{P_{th}}\right) . \tag{4}$$

We calculate the thermal phase shift by solving the equations

$$\frac{d\phi}{dz} = \frac{2\pi}{\lambda_p}\Delta n , \tag{5}$$

$$\frac{dF}{dz} = -\alpha F , \tag{6}$$

where λ_p is the probe wavelength and z is the coordinate along the propagation direction. We integrate this set of equations over the length of the sample cell in the presence of strong saturation. Details of this calculation are outlined in Appendix A. We obtain for the thermal absorption coefficient α_{th} the relation

$$\alpha_{th} = \frac{\varrho C_V \lambda_p \alpha_0 \phi_0}{\pi (dn/dT) F_0} f(F_0/F_S) , \tag{7}$$

where α_0 is the total absorption coefficient at low pump-field fluence, ϕ_0 is the on-axis phase shift at the focus, F_0 is the on-axis pump-field fluence at the focus, F_S is the saturation fluence value and

$$f(x) = \frac{\exp(-x) - 1}{\ln\left(\exp(-\alpha_0 L)(1 - \exp(-x)) + \exp(-x)\right)} . \tag{8}$$

We define the saturation fluence F_S as the value of the field fluence that reduces the absorption by a factor of 2. The peak–valley amplitude of the Z-scan signal determines the magnitude ϕ_0 [12]. By knowing α_{th} and using (4) we can estimate P_{th}.

Figure 1 shows the experimental set-up used to measure the fluorescence quantum yield. The pump field is derived from the output of a dye laser (Continuum ND6000) which is pumped by the second harmonic from a Nd-YAG laser (Continuum Surelite). The dye laser uses rhodamine 6G, emits 5-ns pulses with a spectral width of $0.05\,cm^{-1}$ and is tuned to the maximum of the absorption of the rhodamine 101 solution ($\lambda = 575$ nm). The dye laser is operated in the low-power regime with typical pulse energy of 40 μJ. At the sample, the pulse energy is adjusted to a few micro-joules. A system of mirrors (M) and a 20-cm focal length achromatic lens (L_1) focus the beam onto the sample cell. We measure the spot beam diameter for different positions by moving a blade in the plane perpendicular to the beam direction. By this method we show that the beam is Gaussian with a Rayleigh parameter of 3 cm. Before entering the sample, the beam passes through an optical attenuator (OA) that adjusts the pulse energy. After the sample cell, a lens focuses the light onto a detector (D_1). An analog–digital converter collects the signal from the detector and sends it to a computer for further processing. The computer performs pulse averaging (typical average over 60 pulses). A neutral-density filter (F_1) is used in front of the detector to avoid saturation. The sample cell is a 1-mm path-length glass cell containing a 6×10^{-5} molar solution of rhodamine 101 in ethanol. The use of low concentration mitigates several complicating effects such as concentration quenching and amplified spontaneous emission (ASE) [16, 17]. Rhodamine 101 is remarkable among rhodamine dyes due to its very high fluorescence quantum yield. The dye has become standard for fluorescence and it is a good material for the study of the fluorescence quenching process [18].

For visualizing the nonlinear effect of absorption saturation, we perform an open Z-scan experiment using only the pump light. We measure the sample-cell transmittance as a function of the sample-cell longitudinal position. In the situation of saturation, the total pump-field transmission increases when approaching the focal point.

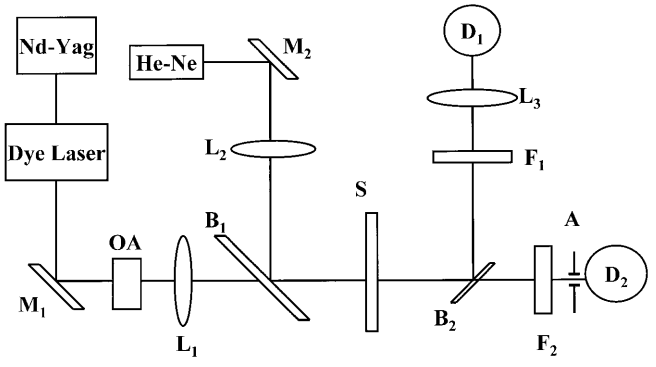

Fig. 1. Experimental set-up consisting of a frequency-doubled Nd-YAG laser (Continuum Surelite, 7-ns pulse duration) that pumps a dye laser (Continuum ND 6000). The dye laser generates the pump field at a fixed wavelength of 575 nm. The pump field passes through the optical attenuator OA, the lens L_1, the beam splitter B_1, the sample cell, the beam splitter B_2, the filter F_1 and finally is focused onto the detector by using the lens L_3. The probe beam is generated by a cw He-Ne laser ($\lambda = 632$ nm). The lens L_2 focuses the probe beam after reflection by the beam splitter B_1. Then, the probe field passes through the beam splitter B_2, the filter F_2 and the aperture A and is monitored by the detector D_2

For the measurement of the TL absorption we use a pump–probe beam configuration (see Fig. 1). A low-power cw He-Ne laser ($\lambda = 632\,\mathrm{nm}$) generates the probe beam. Using an independent lens (L_2) and a beam splitter (B_1) the probe beam is directed collinearly to the pump beam onto the sample cell. We reach a good spatial mode matching between the pump and probe fields by tilting the mirror M_2 and the beam splitter B_1. After the cell the probe light passes through a small aperture (A), a filter that removes the pump light (F_2) and a detector (D_2). The TL signal is averaged on the computer. By removing the aperture, an open Z-scan experiment can be conducted for the TL signal by measuring the total transmission of the probe field in the presence of the thermal lens induced by the pump field.

2 Results

In Fig. 2 we show the pump-field transmission as a function of the sample-cell position (open Z-scan) for three different pump-pulse energies. As expected, the transmission of the single pump beam increases when the sample approaches the focal point, showing a strong saturation of the total absorption. In the same figure we have plotted the probe-field transmission (TL signal open Z-scan) of the same sample. The probe-field transmission does not change with the sample-cell position even for high pulse energies, showing no absorption saturation for the probe field.

In Fig. 3 we show the aperture Z-scan signal (normalized aperture transmittance minus one) for three different values of the pump-pulse energy. In the inset of Fig. 3, we have plotted the peak–valley amplitude as a function of the pump-beam fluence. For a large range of fluence values we observe a linear dependence of the peak–valley amplitude on the pump fluence. This behavior is in contrast to the strong saturation observed for the total absorption. In Fig. 4 we have plotted the total absorption coefficient as a function of the pump-field fluence calculated using Beer's law (2). We also have plotted the thermal absorption coefficient α_{th} calculated using (7) and (8) for the same range of pump-fluence values. For the calculation of α_{th} we use the ethanol

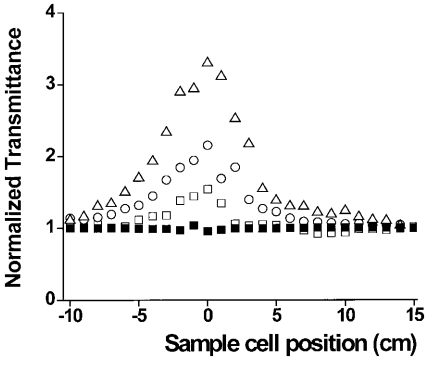

Fig. 2. Normalized sample transmittance for the pump field as a function of the cell position (open Z-scan experiments) of a 6×10^{-5} M ethanol solution of rhodamine 101 for three different pulse energies: 0.05 μJ (*open squares*), 0.1 μJ (*open circles*) and 0.2 μJ (*open triangles*). The *solid squares* correspond to an open Z-scan experiment for the TL signal performed for a pump-pulse energy of 1 μJ. We observe no change of the total transmittance of the probe field for smaller and larger than 1-μJ pump-pulse energies

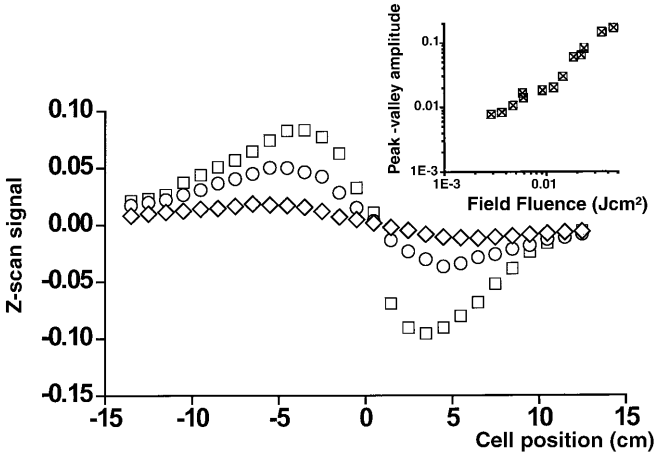

Fig. 3. Z-scan curves for the TL signal for different values of the pump-field pulse energy: 3 μJ (*open squares*), 1.5 μJ (*open circles*) and 0.7 μJ (*open diamonds*). In the *inset* of the figure we show the peak–valley amplitude as a function of the incident pump fluence

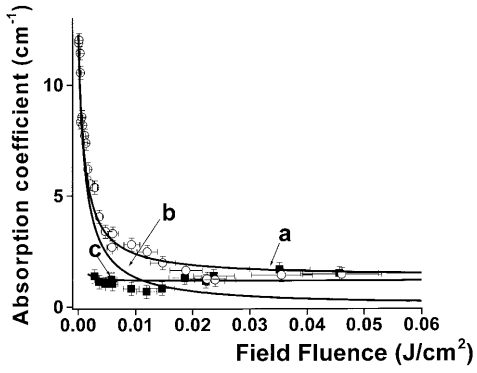

Fig. 4. Total absorption coefficient of a 6×10^{-5} M ethanol solution of rhodamine 101 as a function of the field fluence (*open circles*). The thermal absorption coefficient for the same experimental conditions is also plotted (*solid squares*). The *solid curve* 'b' is calculated using (18) and (19) with the parameters: $T_2 = 30$ fs, $\omega_{0a} = 17\,475\,\mathrm{cm}^{-1}$, $\omega_{0b} = 16\,851\,\mathrm{cm}^{-1}$, $T = 300$ K, $T_3 = 2$ ps, $T_1^* = 2$ ns, $n = 1.3$, $d = 5$ D and $\tau = 5$ ns. The *solid curve* 'a' is calculated using (18) and (19) considering that $T_1 = 0.22 \times 10^{-10}\,\mathrm{s}/F$ and $T_3 = 1.08 \times 10^{-15}\,\mathrm{s}/F$, where F is given in $\mathrm{mJ/cm^2}$. The rest of the parameters are the same as in curve 'b'. The *solid curve* 'c' is calculated using (7), (8) and (18) considering a linear dependence between the induced phase and the incident-field fluence

thermal parameters: $\varrho = 0.789\,\mathrm{g/cm^3}$, $C_{\mathrm{V}} = 87.6\,\mathrm{J/(mol\,°C)}$ and $\mathrm{d}n/\mathrm{d}T = 4 \times 10^{-4}\,°\mathrm{C}^{-1}$ and the measured values $\alpha_0 = 12.5\,\mathrm{cm}^{-1}$ and $F_{\mathrm{S}} = 0.0014\,\mathrm{J/cm^2}$ for the given dye solution. The total absorption coefficient decreases substantially with the pump-field fluence. The thermal absorption coefficient is almost constant for the same fluence values considered.

When increasing the field fluence, the total absorption does not decrease to zero as expected from the simple saturation theory, but approaches the value of the thermal absorption. Using (4) for the calculation of P_{th} and (1) for the calculation of the fluorescence quantum yield, we obtain the result plotted in Fig. 5. The fluorescence quantum yield decreases from a value close to 1 at low fluence to a value five times smaller for fluence values around $0.03\,\mathrm{J/cm^2}$. This means that the fluorescence quenches and that a major amount of the energy absorbed by a highly saturated dye molecule re-

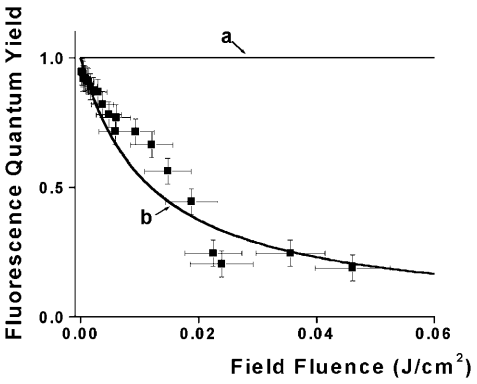

Fig. 5. Fluorescence quantum yield of the 6×10^{-5} M ethanol solution of rhodamine 101 as a function of the pump-field fluence obtained from the data of Fig. 4. The *solid line* 'a' is calculated considering that the relaxation rates are not dependent on the field fluence. The *solid line* 'b' is the theoretical prediction of the proposed model that considers that the relaxation rates depend linearly on the incident-field fluence. All the parameters used in this calculation are the same as in Fig. 4

laxes through a nonradiative process. The solid lines in Figs. 4 and 5 correspond to the theoretical predictions described below.

3 Discussion

The fluorescence and nonradiative transition processes are two different channels for the relaxation of excited molecules. The fluorescence is the result of a quantum spontaneous transition to lower levels. The probability of this transition is mostly determined by the properties of the quantum system itself and not by the external field. Since the fluorescence transition ends with the emission of the absorbed energy, the solvent can not be affected by it. The nonradiative relaxation process is the result of a transition of part of the absorbed energy into the solvent due to the interaction between the dye and the solvent molecules. The solvent molecules are heated, which affects their interaction with the dye molecules. In other words, the absorption process must affect the probability of a nonradiative transition. Below we describe the model for a dye solution in the presence of a high-fluence electromagnetic field that includes both channels of relaxation processes.

The most relevant electronic energy levels for organic dyes in fluid media are the ground state (S_0) and the first electronic excited state (S_1). We can neglect the excited-state absorption (transition $S_1 \rightarrow S_2$) because the cross section for this process in rhodamine dyes is usually more than one order of magnitude smaller than the ground-state absorption cross section (transition $S_0 \rightarrow S_1$). We can also neglect the process of transitions from the single to the triplet levels (transitions $S_1 \rightarrow T_1$) because this process occurs on a time scale much larger than the excitation pulse temporal length used in our experiments. However, we can not neglect the band character of the dye electronic levels. The band structure results from the vibrational and rotational levels of the dye molecule that are highly broadened because of the solvent–solute interaction. To deal with this system, we use the approach described by Mazurenko [19]. Kinoshita and Nishi have successfully used this approach to describe the dynamics of the Stokes effect observed in fluorescence experiments [20, 21]. In this model, the dye molecule and the surrounding solvent molecules constitute an independent quantum system. The energy of this system is a function of the internal coordinates of the dye molecule (R_i) and the external degrees of freedom of the solvent molecules (configurational coordinates R). The internal degrees of freedom define the electronic ground and excited states of the system. The interaction with the solvent molecules changes the energy values of the electronic states for each solute molecule. For fixed values of the internal coordinates R_i, the level energies become a function of the external coordinates R, and so does the resonant frequency of the quantum transition. The Franck–Condon principle gives the value of the transition frequency

$$\omega_0(R) = (U_2(R) - U_1(R))/\hbar\,, \tag{9}$$

where $U_1(R)$ and $U_2(R)$ are the ground and excited energy values, respectively. Figure 6 depicts the band model of the dye solution. The functions $U_1(R)$ and $U_2(R)$ are represented by adiabatic potential curves with minimal values that are the minimal equilibrium values after relaxation of the active centers [19–21]. In thermal equilibrium the energy of an individual active center is determined by the Boltzmann distribution around the minimum of these potential curves. If an electromagnetic pulse drives the system from the equilibrium, the interaction between the solute and solvent molecules restores the equilibrium after the cross-relaxation time T_3. When considering the interaction of the molecular system with an external electromagnetic field, the system can be treated as an inhomogeneously broadened ensemble of Franck–Condon systems with resonant frequencies given by (9). For each excited Franck–Condon state, spontaneous fluorescence transition to the ground state occurs at rate $A(\omega_0)$. Besides the cross-relaxation process inside the band, nonradiative relaxation transitions to the ground level occur at rate $1/T_1$. The

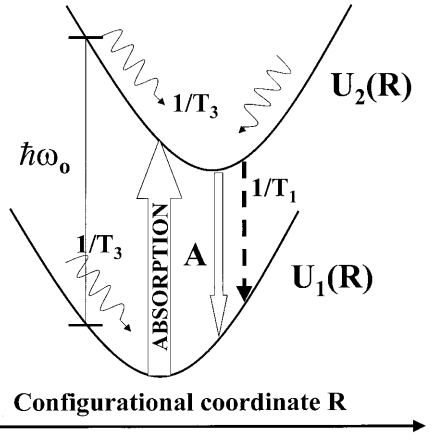

Fig. 6. Adiabatic potential curves for the ground and excited states of the dye solution as function of the configurational coordinate R. Different active centers are at different coordinates R. The resonant frequency is a function of R according to (9). At equilibrium the distribution is Boltzmann. The relaxation process along each band has a characteristic cross-relaxation time T_3. The processes of absorption, fluorescence and nonradiative relaxation take place along the whole band. The fluorescence occurs at rate $A(\omega_0)$ and the nonradiative relaxation from the excited to the ground band occurs at rate $1/T_1$

rate equations for this system can be written as

$$\frac{\mathrm{d}n_1}{\mathrm{d}t} = (n_2 - n_1)\frac{\sigma F_0}{2\hbar\omega\tau h_0(\omega_0)} - \frac{n_1}{T_3} + \frac{n_2}{T_1} + A(\omega_0)n_2 + \frac{g_1(\omega_0)}{T_3}N_1\,, \tag{10}$$

$$\frac{\mathrm{d}n_2}{\mathrm{d}t} = -(n_2 - n_1)\frac{\sigma F_0}{2\hbar\omega\tau h_0(\omega_0)} - \frac{n_2}{T_3} - \frac{n_2}{T_1} - A(\omega_0)n_2 + \frac{g_2(\omega_0)}{T_3}N_2\,, \tag{11}$$

$$\frac{\mathrm{d}N_1}{\mathrm{d}t} = \int_0^\infty (n_2 - n_1)\frac{\sigma F_0}{2\hbar\omega\tau h_0(\omega_0)}\mathrm{d}\omega' + \frac{N_2}{T_1} + A_{\mathrm{ef}}N_2\,, \tag{12}$$

$$\frac{\mathrm{d}N_2}{\mathrm{d}t} = -\int_0^\infty (n_2 - n_1)\frac{\sigma F_0}{2\hbar\omega\tau h_0(\omega_0)}\mathrm{d}\omega' - \frac{N_2}{T_1} - A_{\mathrm{ef}}N_2\,, \tag{13}$$

where n_1 and n_2 are the populations of the ground and excited Franck–Condon states, respectively; $N_1 = \int_0^\infty n_1 \mathrm{d}\omega'$ and $N_2 = \int_0^\infty n_2 \mathrm{d}\omega'$ are the total populations of the ground and excited electronic bands, respectively; $\sigma = 8\omega d^2 T_2/(3\sqrt{\pi}nc\varepsilon_0\hbar)$ is the peak-absorption cross-section absorption; n is the solution refraction index; c is the speed of light; ε_0 is the vacuum dielectric permeability; d is the averaged-over-orientations dipole moment; T_2 is the phase relaxation time; $h_0(\omega_0) = 1 + T_2^2(\omega - \omega_0)^2$; ω is the incident-field frequency; $A_{\mathrm{ef}} = \int_0^\infty A(\omega')n_2\mathrm{d}\omega'/N_2$ and $g_1(\omega_0)$ and $g_2(\omega_0)$ are the population distribution functions for the ground and excited states, respectively. In (10) through (13) we have considered that the incident electromagnetic pulse is Gaussian with pulse duration equal to τ.

The distributions $g_1(\omega_0)$ and $g_2(\omega_0)$ are determined by the active center distributions in ground and excited states and depend on the shape of the potential curves $U_1(R)$ and $U_2(R)$. For these functions we use the approach proposed by Kinoshita and Nishi based on Onsager's cavity model [21]. In Appendix B we show details of this calculation. From this model we obtain

$$g_{1,2}(\omega_0) = \sqrt{\gamma/\pi}\exp(-\gamma(\omega_{1,2}^{(0)} - \omega_0)^2)\,, \tag{14}$$

where $\gamma = \hbar c/(\omega_{\mathrm{SS}}kT)$, ω_1^0 is the peak absorption frequency, $\omega_2^0 = \omega_1^0 - \omega_{\mathrm{SS}}$, ω_{SS} is the Stokes shift, k is the Boltzmann constant and T is the temperature.

We solve (10) through (13) in the stationary approximation. At room temperature the cross-relaxation rate $(1/T_3)$ is in the range of $10^{12}\,\mathrm{s}^{-1}$ and the fluorescence rate A and $(T_1^*)^{-1}$ are in the range of $10^9\,\mathrm{s}^{-1}$. The stationary approximation is well justified for an electromagnetic pulse of $5\times10^{-9}\,\mathrm{s}$ [22]. Solving (10) through (13) in the stationary approximation, we obtain for the population difference $\Delta n = n_2 - n_1$ and for N_2 the relations

$$\Delta n(\omega_0) = \frac{(g_1(\omega_0) + g_2(\omega_0)((T_1^* - T_3)/(T_1^* + T_3)))N_2 - g_1(\omega_0)N}{1 + \sigma F_0 T_1^* T_3/(\hbar\omega\tau h_0(T_1^* + T_3))}\,, \tag{15}$$

$$N_2 = \frac{NG_1\sigma F_0 T_{1\mathrm{ef}}^*/(2\hbar\omega\tau)}{1 + (G_1 + G_2)F_0\sigma T_{1\mathrm{ef}}^*/(2\hbar\omega\tau)}\,, \tag{16}$$

where $N = N_1 + N_2$; $T_1^* = T_1/(1 + AT_1)$; $T_{1\mathrm{ef}}^* = T_1/(1 + A_{\mathrm{ef}}T_1)$; $G_1 = \int_0^\infty g_1(\omega')/(h_0(\omega') + \sigma T_1^* T_3 F_0/(\hbar\omega\tau(T_1^* + T_3)))\mathrm{d}\omega'$ and $G_2 = \int_0^\infty g_2(\omega')((T_1^* - T_3)/(T_1^* + T_3))/(h_0(\omega') + \sigma T_1^* T_3 F_0/(\hbar\omega\tau(T_1^* + T_3)))\mathrm{d}\omega'$. The absorption coefficient is given by

$$\alpha = -\int_0^\infty \frac{\sigma\Delta n(\omega')}{h_0(\omega')}\mathrm{d}\omega'\,, \tag{17}$$

From (15), (16) and (17) we obtain

$$\alpha = \frac{\alpha_0}{1 + F_0/F_{\mathrm{S}}}\,, \tag{18}$$

where $\alpha_0 = \sigma N G_1$ and

$$F_{\mathrm{S}} = \frac{2\hbar\omega\tau}{\sigma T_{1\mathrm{ef}}^*(G_1 + G_2)}\,. \tag{19}$$

We calculate the fluorescence quantum yield by dividing the amount of fluorescence photons per second ($A_{\mathrm{ef}}N_2$) by the amount of absorbed photons per second ($F_0\alpha/(2\tau\hbar\omega)$). After simple algebraic calculation we obtain

$$\phi_{\mathrm{f}} = \frac{A_{\mathrm{ef}}T_1}{1 + A_{\mathrm{ef}}T_1}\,. \tag{20}$$

The saturation effect reduces the total absorption to zero if the parameters T_1 and A do not change during the field–matter interaction. In this situation, the presence of high field fluence does not affect the fluorescence quantum yield as defined by (20). We propose that the probability of nonradiative transitions $(1/T_1)$ increases with the field fluence while the spontaneous fluorescence probability A remains constant. The probability of a nonradiative transition is determined by the interaction between the dye molecules and the surrounding solvent molecules. This relaxation process depends on the temperature (see for example [23]). Increasing the external field fluence reduces the characteristic times of translational and rotational displacements of the surrounding solvent molecules because of the larger amount of energy converted into heat. The spontaneous fluorescence is a quantum characteristic of the dye molecule itself and does not vary through the solute–solvent interaction. Considering that the nonradiative relaxation rate increases linearly with the field fluence, when increasing the external field fluence we will have

$$A_{\mathrm{ef}}T_1 \to 0\,, \quad \text{and} \quad \phi_{\mathrm{f}} \to 0\,. \tag{21}$$

The relation (21) means that the fluorescence process quenches and that the relative amount of the absorbed energy that is converted into heat increases. This model also predicts that the absorption coefficient does not approach zero when increasing the field fluence. It approaches the value of the thermal absorption (see below).

For the sake of simplicity, in the calculations below we suppose $T_1^* = T_{1\mathrm{ef}}^*$ for any value of the resonant frequency ω_0 within the molecular band. Using (18) with the parameters: $T_2 = 30\,\mathrm{fs}$, $\omega_{0\mathrm{a}} = 17\,475\,\mathrm{cm}^{-1}$, $\omega_{0\mathrm{b}} = 16\,851\,\mathrm{cm}^{-1}$, $T = 300\,\mathrm{K}$, $T_3 = 2\,\mathrm{ps}$, $T_{1\mathrm{ef}}^* = 2\,\mathrm{ns}$, $n = 1.3$, $d = 6\,\mathrm{D}$ and $\tau = 5\,\mathrm{ns}$ we calculate the absorption coefficient in the situation of fixed values of the relaxation rates. The value of T_2 is in the

range of 7 to 90 fs measured for different rhodamine solutions in four-wave-mixing experiments [24]. The value of ω_{0a} corresponds to the peak absorption of rhodamine 101. The difference $(\omega_{0b} - \omega_{0a})$ correspond to the Stokes shift for rhodamine 101 ($\omega_{SS} = 624\,\mathrm{cm}^{-1}$). The value for T_3 is in good agreement with the characteristic time of translational and rotational displacements of liquid molecules at room temperature [25]. The value of T_{1ef}^* is in good agreement with previous reported values for similar systems [26]. The result of this calculation is depicted by the solid curve 'b' of Fig. 4. For fluence values larger than $0.004\,\mathrm{mJ/cm}^2$ the calculation does not reproduce the experimental results. The calculated absorption coefficient decreases to zero, in disagreement with the experimental results that show stabilization of the absorption around the thermal absorption value. However, this discrepancy can be corrected by using the same equation (18) with the range of experimental fluence values $0.0001\,\mathrm{J/cm}^2 < F_0 < 0.05\,\mathrm{J/cm}^2$ and the relaxation times T_1 and T_3 being governed by

$$T_1 = 2.2 \times 10^{-11}\,\mathrm{s}/F_0 \quad \text{and} \tag{22a}$$

$$T_3 = 1.08 \times 10^{-15}\,\mathrm{s}/F_0\,, \tag{22b}$$

where F_0 is given in $\mathrm{J/cm}^2$. For the given experimental situation, these relaxation times change in the ranges $2.2 \times 10^{-7}\,\mathrm{s} > T_1 > 0.43 \times 10^{-9}\,\mathrm{s}$ and $10^{-12}\,\mathrm{s} > T_3 > 2 \times 10^{-14}\,\mathrm{s}$. For $A_{ef} = 0.5 \times 10^9\,\mathrm{s}^{-1}$, we obtain for the relaxation time: $2 \times 10^{-9}\,\mathrm{s} > T_{1ef}^* > 0.35 \times 10^{-9}\,\mathrm{s}$. We calculate the absorption using (18) taking into account the relations (22a) and (22b). The rest of the parameters are the same as in the previous calculation of curve 'b'. The result is shown by curve 'a' of Fig. 4. In the same figure the solid curve c is the calculation of the thermal absorption using (7), where we have considered a linear proportionality between the induced phase and the incident-field fluence.

Using (20) and relations (22a) and (22b), we calculate the dependence of the fluorescence quantum yield on the pump-field fluence. The result is given by curve 'b' in Fig. 5. The rest of the parameters are the same as in the calculation of Fig. 4. If again we consider that the relaxation times do not depend on the field fluence, we obtain the curve 'a' that shows a constant value of the fluorescence quantum yield; a result that clearly does not fit the experimental observations.

In the model we have used the stationary approximation. However, conclusions similar to ones presented here can be obtained by a direct numerical integration of (11) through (14).

The model explains well all the observed phenomena: the initial reduction of the absorption coefficient at moderate fluence values and its stabilization at high fluence, the quenching of the fluorescence and the lack of saturation of the thermal absorption coefficient.

4 Conclusions

We have investigated the influence of the saturation of absorption on the fluorescence process. We show that the fluorescence quantum yield decreases when increasing the external field fluence. This is the result of the combination of two effects: the saturation of the absorption that reduces the amount of energy absorbed by the dye solution and the competition between the fluorescence and the nonradiative relaxation channels from the excited state. The amount of excited molecules relaxing through a fluorescence process decreases with the field fluence. However, the amount of excited molecules that give their energy up to the solvent molecules through a nonradiative channel remains almost unaltered when increasing the field power. Three experimental facts support this interpretation: the lack of saturation of the thermal absorption, the stabilization of the total absorption around the value of the thermal absorption and the quenching of the fluorescence.

Acknowledgements. We thank Dr. N. Melikechi and Dr. R. Pradhan from the Applied Optics Center of Delaware, Delaware State University, Dover, Delaware, US, for the critical reading of the manuscript and enlightening discussions. We also gratefully acknowledge the financial support from the Consejo Nacional de Investigaciones Científicas y Tecnológicas (CONICIT), Caracas, Venezuela (Grant G-97000593).

Appendices

Appendix A

We solve (5) and (6) in the presence of saturation of the absorption. Combining (6) and (18), we have

$$\frac{\mathrm{d}F}{\mathrm{d}z} = -\frac{\alpha_0 F}{1 + F/F_S}\,. \tag{A.1}$$

The integration of this equation along the path length of the sample cell gives

$$F = \frac{F_0}{1 - \exp(-F_0/F_S) + \exp(\alpha_0 L - F_0/F_S)}\,, \tag{A.2}$$

where L is the length of the sample cell and F_0 is the external field fluence at the entry of the sample cell. Combining (4), (5) and (A.2) we obtain for the induced thermal phase shift ϕ_0

$$\frac{\mathrm{d}\phi_0}{\mathrm{d}z} = \frac{\pi\alpha_{th}F_0}{\lambda_p \varrho C_V}\left(\frac{\mathrm{d}n}{\mathrm{d}T}\right)\frac{1}{1 - \exp(-F_0/F_S) + \exp(\alpha_0 z - F_0/F_S)}\,. \tag{A.3}$$

We integrate (A.3) again over the sample-cell path length. From the obtained expression we can deduce (7) for the thermal absorption coefficient α_{th}.

Appendix B

In this appendix we calculate the distribution functions of the ground and excited states using the configurational coordinate (CC) model. We start from the free-energy expression for the electronic and excited states after Kinoshita and Nishi [21]. As a configurational coordinate they choose the reaction field of the medium defined in the dielectric theory after Zwan and Hynes [27]. This theory is based on the Onsager cavity model. The Onsager cavity model treats the molecule as

a point dipole buried within a spherical cavity in a continuous dielectric medium. The free energies are expressed in the following form:

$$U_1 = U_1^0 + CQ^2 \,, \tag{B.1}$$

$$U_2 = U_2^0 + C(Q - Q_0)^2 \,, \tag{B.2}$$

where $U_{1,2}^0$ are the minimal values of the free energies of the ground and excited states, respectively; $Q = R - R_1^{\mathrm{eq}}$ and $Q_0 = R_1^{\mathrm{eq}} - R_2^{\mathrm{eq}}$; R_1^{eq} and R_2^{eq} are the equilibrium reaction fields for the relaxation in the electronic and ground states, respectively and $C = \hbar\omega_{\mathrm{SS}}/(2Q_0^2)$.

Using (B.1) and (B.2) we obtain the relation between the configurational coordinate Q and the resonant frequency ω_0

$$Q = \hbar(\omega_1^0 - \omega_0)/(2CQ_0) \,, \tag{B.3}$$

with

$$\omega_1^0 = (U_2^0 - U_1^0 + CQ_0^2)/\hbar \,. \tag{B.4}$$

At low field fluence, the absorption spectrum has a maximum at ω_1^0. At thermal equilibrium the distribution is Boltzmann. Then, the distribution functions $g_{1,2}$ can be written as

$$g_{1,2}(\omega_0) = g_{1,2}^0 \exp(-U_{1,2}/kT) \,, \tag{B.5}$$

where the constants $g_{1,2}^0$ are determined from the normalization condition

$$\int_0^\infty g_{1,2}(\omega_0)\mathrm{d}\omega_0 = 1 \,. \tag{B.6}$$

Using (B.1), (B.2) and (5) we obtain (14).

References

1. J.H. Brannon, D. Magde: J. Phys. Chem. **82**, 705 (1978)
2. J. Shen, R.D. Snook: Anal. Proc. **26**, 27 (1989)
3. D. Magde, J.H. Brannon, T.L. Cremers, J. Olmsted III: J. Phys. Chem. **83**, 696 (1979)
4. A.V. Butenin, B.Ya. Kogan, N.V. Gundobin: Opt. Spectrosc. **47**, 568 (1979)
5. M. Fisher, J. Georges: Chem. Phys. Lett. **260**, 115 (1996)
6. M.D. Galanin, B.P. Kirsanov, Z.A. Chizhikova: JETP Lett. **9**, 304 (1969)
7. P. Peretti, P. Ranson: C. R. Acad. Sci. Ser. B **270**, 757 (1970)
8. D.J. Bradley, M.H.R. Huttchinson, H. Koester, T. Morrow, G.H.C. New, M.S. Petty: Proc. R. Soc. London Ser. A **328**, 97 (1972)
9. S. Mory, D. Leupold, R. Konig: Opt. Commun. **6**, 394 (1972)
10. B.A. Bushchuk, A.N. Rubinov: Opt. Spektrosk. **53**, 1031 (1982)
11. M. Sheik-Bahae, A.A. Said, E.W. Van Stryland: Opt. Lett. **14**, 955 (1989)
12. M. Sheik-Bahae, A.A. Said, T.H. Wei, D.J. Hagana, E.W. Van Stryland: IEEE J. Quantum Electron. **QE-26**, 760 (1990)
13. H. Ma, A.S.L. Gomes, C.B. de Araújo: Appl. Phys. Lett. **59**, 2666 (1991)
14. M. Sheik-Bahae, J. Wang, R. De Salvo, D.J. Hagan, E.W. Van Stryland: Opt. Lett. **17**, 258 (1992)
15. J. Castillo, V.P. Kozich, A. Marcano O.: Opt. Lett. **19**, 171 (1994)
16. A.A. Hnilo, O.E. Martinez, E.J. Quel: IEEE J. Quantum Electron. **QE-22**, 20 (1986)
17. I.A. McIntyre, M.H. Dunn: Opt. Commun. **50**, 169 (1984)
18. K.H. Drexhage: J. Res. Nat. B. Stand. A **80**, 421 (1976)
19. Y. Mazurenko: Opt. Spectrosc. **48**, 388 (1980)
20. S. Kinoshita, N. Nishi, T. Kushida: Chem. Phys. Lett. **134**, 605 (1987)
21. S. Kinoshita, N. Nishi: J. Chem. Phys. **89**, 6612 (1988)
22. C. Jensen: *Pulsed dye laser gain analysis and amplifier design*. In High Power Dye-Lasers, Vol. 65, ed. by F.J. Duarte (Springer, New York 1991) p. 45
23. W. Ware, S.K. Lee, G.J. Brant, P. Chow: J. Chem. Phys. **54**, 4729 (1971)
24. B.S. Neporent, A.G. Spiro: Opt. Spectrosc. **78**, 25 (1995)
25. F. Laermer, T. Elsaesser, W. Kaiser: Chem. Phys. Lett. **156**, 381 (1989)
26. E.N. Victorova, I.A. Gofman: Zh. Fiz. Khim. **39**, 2643 (1965)
27. G. Van der Zwan, J.T. Hynes: J. Phys. Chem. **89**, 4181 (1985)